DEVELOPMENT OF MIRROR CELLS FOR A SATELLITE BORN SOLAR TELESCOPE

J. Bischoff[1], B. Grauf[1], J. Staub[1], A. Gandorfer[1], J. Woch[1], S. Clark[2], M. Zimmermann[3], A. Kolb[3], B. Metz[3], P. Rucks[4]

[1] Max-Planck Institut für Sonnensystemforschung Göttingen, [2] Stein-Engineering Ulm, [3] Cassidian Optronics Oberkochen, [4] Carl-Zeiss Jena

ABSTRACT

The paper discusses the optical design, the stray light and surface roughness requirements and the opto-mechanical design of the mirror cells for a space born solar telescope. Some required performance parameters and theoretical simulations are given and it is shown by means of experimental results that the most ambitious demands are met.

1. INTRODUCTION

The development of the mirror cells for an ESA/NASA Solar Orbiter mission telescope is presented. This mission is dedicated to solar and heliospheric physics and was selected as the first medium-class mission of ESA's Cosmic Vision 2015-2025 Program. The space craft will carry a scientific payload of various instruments. One of the imaging remote-sensing instruments onboard will be the Polarimetric and Helioseismic Imager (PHI). The PHI instrument will provide high-resolution and full-disc measurements of the photospheric vector magnetic field and line-of-sight (LOS) velocity in the visible wavelength range. The LOS velocity maps will allow detailed helioseismic investigations of the solar interior, in particular of the solar convection zone. PHI will address and resolve basic questions in solar physics by studying the sun at high resolution from close up and from high latitudes up to 35°. It will be composed of two telescopes. The off-axis Ritchey-Chrétien High Resolution Telescope (HRT) will image a fraction of the solar disk at a resolution reaching 150 km at perihelion. The refractor Full Disk Telescope (FDT) will be able to image the full solar disk at all phases of the orbit. Each telescope will have its own Polarization Modulation Package (PMP) located early in the optical path in order to minimize polarization cross-talk effects. Polarimetry at a signal-to-noise level of 10^3 is baselined for PHI. The HRT and the FDT will sequentially send light to a Fabry-

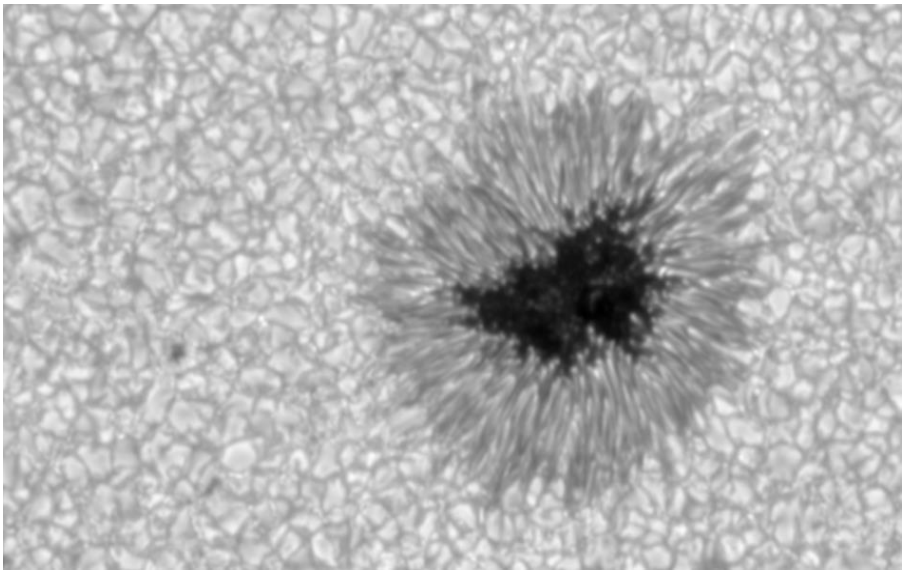

Figure 1: Image of the photosphere of the sun

Perot filtergraph system (~ 100 mÅ spectral resolution) and on to a 2048 × 2048 pixel CMOS sensor. An image of the sun's photosphere is shown in figure 1. A sun spot can be seen in the right center. Furthermore, the granules are clearly resolved which possess diameters of a few hundred up to 1000 km.

The following model philosophy was decided for the mirror cell development. First, a so-called qualification model (QM) was built to prove the mechanical, thermal and optical properties of the mirrors as predicted in the FE-analysis. This included for example vibration tests beyond the anticipated loads during lunch and operation in order to prove the robustness of the designs. After successful completion of these tests, two flight models (FM) have been built which are foreseen to be integrated in the flight model and the so-called flight spare of the PHI instrument.

This paper is structured as follows. In the next section, the optical design of the telescope is presented and the wave front budget is established for both mirrors to ensure the required optical performance under operational conditions. The first interferometric measurements show nearly perfect surfaces. The surface roughness of the mirrors and its impact on the optical imaging is discussed in section 3. This is followed by the presentation of the opto-mechanical design of the mirror cells. Here, some results of the finite element analysis are presented and compared with the results of the vibration measurements. A brief summary concludes this contribution.

2. OPTICAL DESIGN AND PERFORMANCE

The main focus of this paper is on the optical and opto-mechanical development of the PHI-HRT.

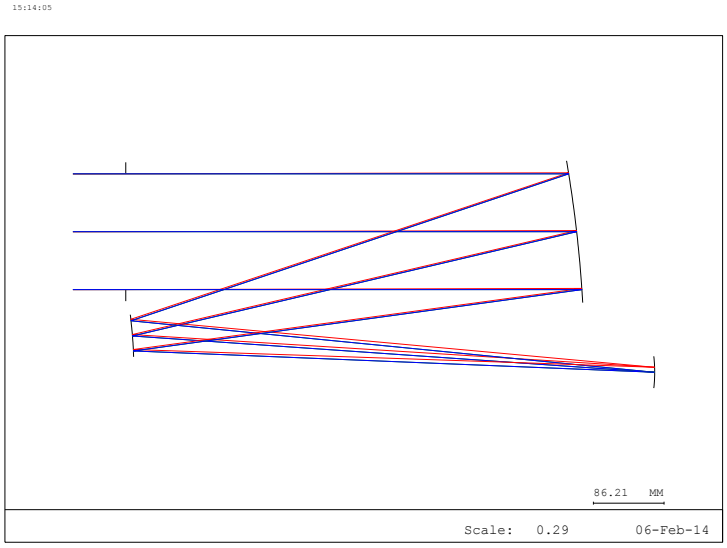

Figure 2: Optical Design of the HRT telescope

A sketch of the optical design is shown in figure 2. The telescope is formed by a primary concave and a secondary convex mirror. The entrance aperture of the system is 140 mm. The primary is almost parabolic while the secondary is hyperbolic. The telescope has a focal length of 2475 mm. The instrument operates on the Fe-line at 617.3 nm with a spectral bandwidth of 30 nm. The field is rectangular with a size of ±0.14 degrees. Since the telescope has no real intermediate focus, the radiation energy entering the entrance pupil has to be stopped down by a series of vignetting stops. The required resolution is about 1 arcsec resulting in a maximum total wave front error of λ/25. This imposes extreme challenges on the optical and mechanical development. In order to assess the effects of manufacturing as well as thermal and structural effects on the optical performance, a tolerance analysis was run resulting in limits for the allowed decentering, axial distance change, tilt and surface deformation of the telescope. Due to the planned elliptical orbit around the sun, the telescope has to be fully operational in a temperature range from -30°C (Aphelion) through +90°C (Perihelion). In order to take all these effects into account, error budgets for the various contributions to wave-front degradation such as temperature change, mounting errors, gravity release and mostly important manufacturing, i.e., polishing related deviations of the optical surfaces from its ideal shape have

been set up for both mirror cells (see Table 1). Evidently, the total budget with gravity release for the M1 is slightly over specification (WFE < 25 nm). However, it should be pointed out here that on the one hand, the worst case of out-of-plane gravity (meaning horizontal mounting) of 16 nm has been assumed. The more realistic in-plane case for gravity release provides only 2 nm. On the other hand, a rather conservative measurement accuracy of 10 nm was assumed. Taking this into account, the total budget drops easily below the 25 nm WFE requirement.

Table 1: Wave-front error budgets for the M1- (left hand side) and M2-mirror (right hand side)

Contributer	WFE [nm rms]
Operational Temperature	2,4
Mounting Error	0,082
Gravity Release	16
Measurement Accuracy	10
Vibration	3
Manufacturing	19
Sum w/o Gravity Release	21,8
Sum w/ Gravity Release	27,1

Contributer	WFE [nm rms]
Operational Temperature	6
Mounting Error	10,2
Gravity Release	0,2
Measurement Accuracy	10
Vibration	3
Manufacturing	19
Sum w/o Gravity Release	24,7
Sum w/ Gravity Release	24,7

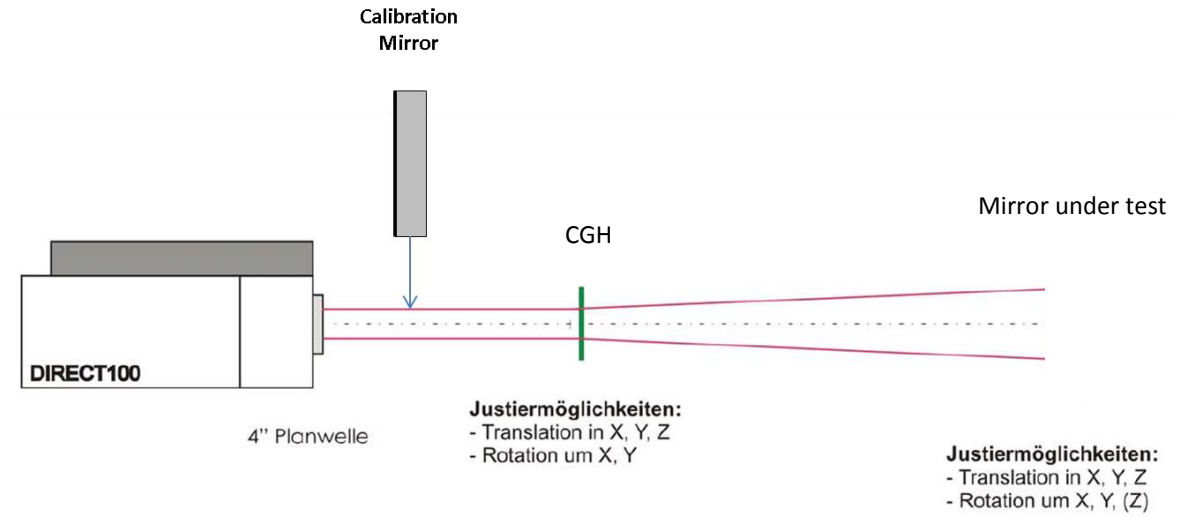

Figure 3: CGH based Null-Interferometry Setup for M1

Furthermore, the mirror surfaces have been measured optically by means of so-called Null-interferometry where a computer generated hologram (CGH) is used to adapt the wavefront to the aspherical surface shape. The basic experimental setup for the M1 mirror is shown in figure 3. A similar setup was applied for M2 taking its convex surface into account.The interferogram of the M1-QM mirror after vibration testing (see section 4.1) is shown in figure 4. The measured root mean square (rms) wave-front error (WFE) is 23.9 nm. The rather sharp gradients in the center indicate the fixing points of the bipod-Zerodur mounts. It seems that subtle settling effects occurred during the vibration tests. This was partly confirmed by minimal differences between the sine sweeps performed before and after the 0dB-random-vibration test of the vertical axis.

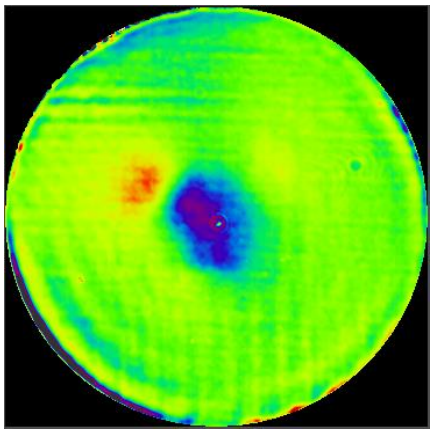

Figure 4: Interferogram of the M1-QM

By means of further improvements during the manufacturing and assembling procedures such as common grinding of the insert and mirror cones, the performance of the mirror was greatly improved. The interferograms of the FM's are depicted in figure 5 for M1 and in figure 6 for M2. Clearly, excellent rms-wave-front error values as low as about 17 nm and 19 nm, respectively, could be achieved. Thus, the requirements established for the error budget (manufacturing + vibration) could be fulfilled with a comfortable margin. Moreover, the subtle deviations of the surface due to the vibration loads as observed for the QM could be avoided for the FM-mirrors as nicely can be shown in figure 7 for the M1 mirror opposing the interferograms after ion beam figuring (IBF), after thermal cycling and after vibration. The wave front error is only slightly degraded and there are no significant changes of the shape to be observed.

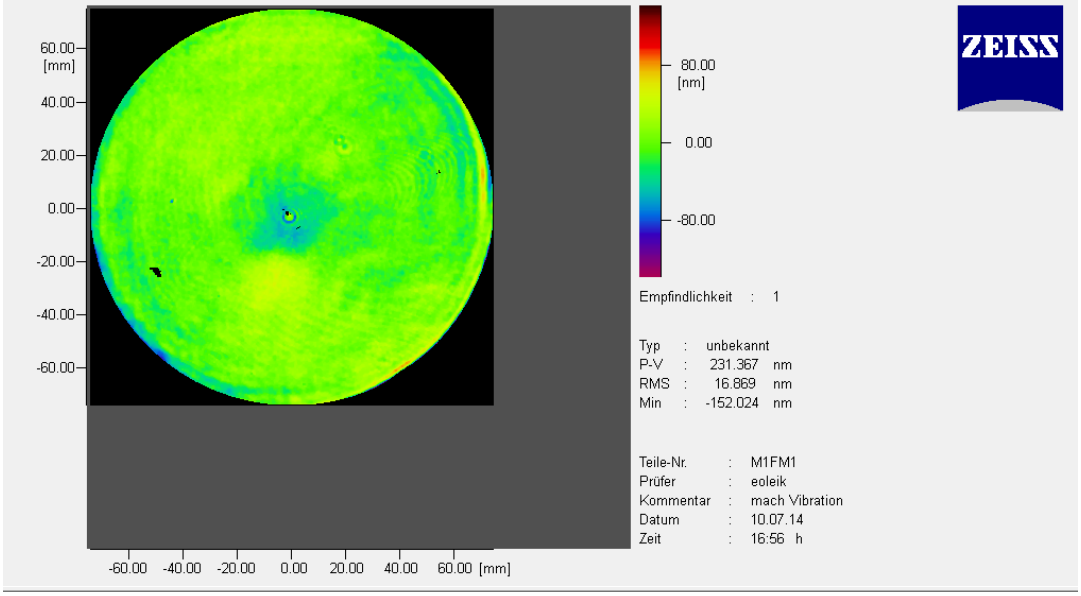

Figure 5: Interferogram and Zernike Coefficients for the M1-FM mirror after vibration

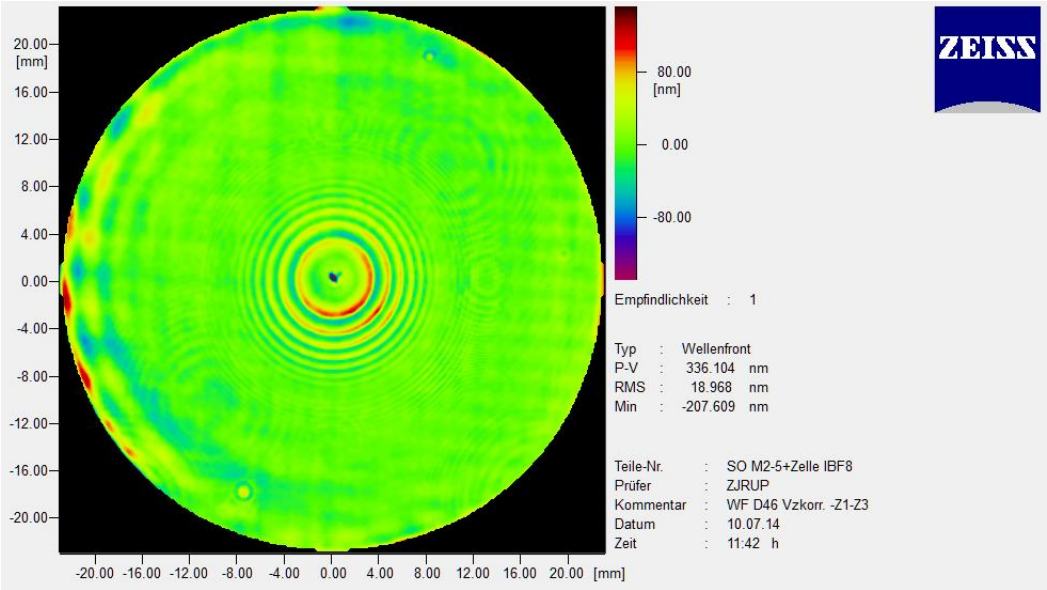

Figure 6: Interferogram for the M2-FM mirror after vibration

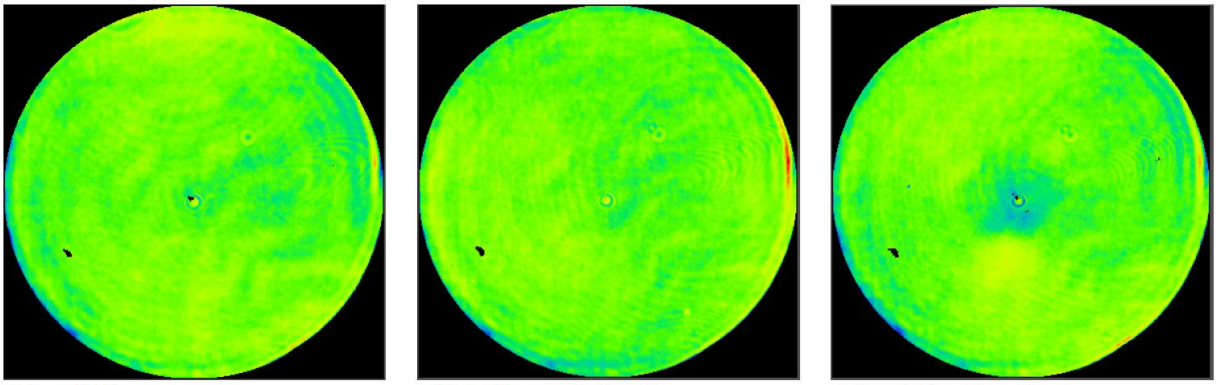

After IBF
rms WFE = 14.8 nm

After Thermal Cycling
rms WFE = 13.8 nm

After Vibration Test
rms WFE = 16.9 nm

Figure 7: Interferograms for M1 – FM (after IBF, after thermal cycling and after vibration test)

Then, the measurement data ("int"-format) were fed into an optical design software and a performance analysis was run. In this way, it could be verified that the as-built telescope is able to meet the requirement of Strehl > 0.8 if adjusted appropriately. Furthermore, diffraction MTF's for the "as built" telescope systems have been simulated for the high qualitative mirrors as presented above (figure 8, left). For comparison, MTF's for a system with an out-of-spec secondary mirror in an earlier polishing iteration showing severe wave front perturbations near the rim (figure 8, right) and a band-rms (MSF) of about 7 nm (see section 3) have been also simulated. While the MSF-drop for the high-quality system is only about 1%, the degraded system shows about 5% which nicely confirms the estimation of figure 9. This is not acceptable due to the already low contrast in the areal object to be observed (see figure 1). Please, note that the cut-off frequency is correctly simulated with $R = \frac{2\rho_P}{\lambda f'} = \frac{140\ mm}{617nm \cdot 2475mm} \approx 90\ mm^{-1}$.

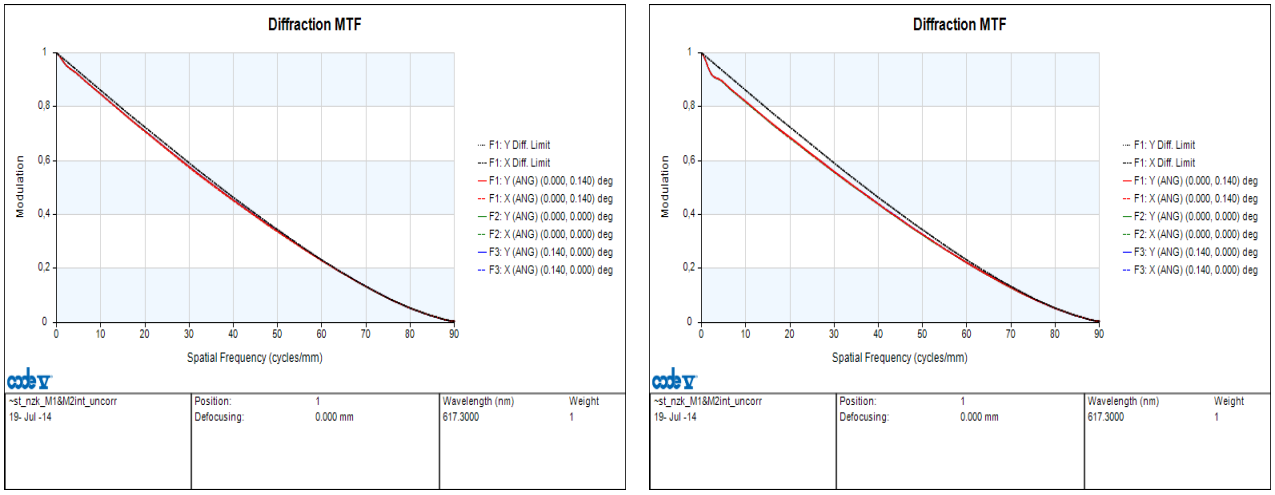

Figure 8: Modeled diffraction MTF for a telescope assembled from the high quality mirrors (Figure 5 and Figure 6) –left and a telescope with a degraded M2 -right

3. SURFACE ROUGHNESS

Surface roughness is particularly critical for reflective optical systems because it directly translates into stray light flare [1]. There are various contributors to stray light in the HRT part of the PHI instrument. Surface roughness is best discussed in terms of the power spectrum density (PSD). Optical fabrication techniques for spheres have part-to-tool geometry that can generate long scale length surface undulations, referred to as form errors, and also surface fracture mechanics that lead to short spatial scale length undulations, referred to as micro-roughness and scatter. Therefore, usually only two numbers are specified: the figure or form deviation in terms of Nijboer Zernike polynomials and the surface roughness either given as rms roughness. Form errors have been discussed in the previous section. Surface (high frequency) roughness is usually measured by means of micro-interferometry (see below).

Besides, the HRT mirror surfaces are highly aspheric. They are processed to nanometer accuracy with modern single diamond turn and polishing techniques. The final polishing steps are usually done with ion beam figuring. Thus, they are more prone to residual periodic surface undulations that are commonly referred to as ripple, or mid-spatial frequency (MSF) errors. These errors may result in considerable contrast deteriorations which are particular harmful for the observation of extended objects such as the sun. Consequently, another criterion is required to specify the impact of these surface-MSF's on the image quality. The contrast drop due to MSF roughness σ can be approximated by means of $\mathrm{MTF}_{\mathrm{MSF}} = \exp\left[-\left(4\pi/\lambda\right)^2 \cdot \sum_i \sigma_i^2\right]$ where σ is the rms roughness [2].

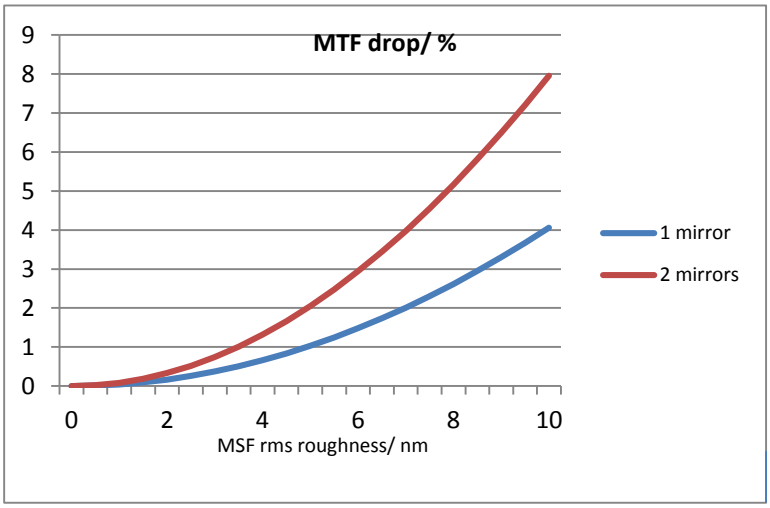

Figure 9: Predicted MTF drop for two-mirror telescope due to MSF roughness

This behavior is shown in figure 9. Therefore, a permitted contrast drop of 0.5% results in 2…2.5 nm MSF roughness for the mirror surface. In addition, the high-spatial frequency roughness is adapted to the micro-interferometer ranges, namely < 1.5 nm for 0.4/mm through 20/mm (2.5x magnification), and <0.8 nm for 5/mm through 500/mm (40x). Experimental data for the two magnification ranges have been collected and the resulting PSD curves are shown in figure 10 (blue and red). Then, a Harvey-Shack BSDF (bidirectional scatter distribution function) [1,3] was fitted to it with parameters b0 = 80, S = -2.8 & L = 0.001 (green).

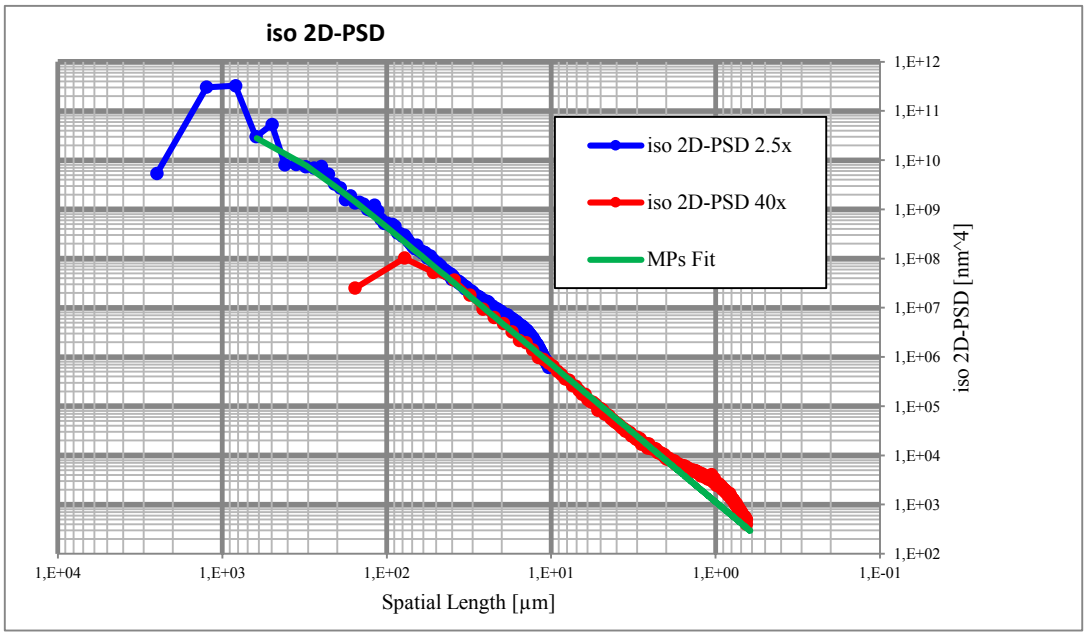

Figure 10: Measured and Model PSD

Following, a stray light simulation of the optical system was run with the Photon Engineering FRED simulator [4]. Hereby, additional assumptions have also been included in the simulations. For instance, mechanical parts such as mountings or stops have been modeled as black Lambertian scatterers meaning that the incident light is scattered uniformly in all directions with considerably reduced reflectivity of 5 to 10 %. FRED offers a predefined element called Black Lambertian for this purpose. Moreover, particulate contamination was taken into account via an equivalent surface roughness (were the particle effect is translated in additional rms-surface roughness) as well as by means of separate particle BSDF's. According to ESA cleanliness specifications, a particle contamination cleanliness level CL350 equivalent to 500 ppm has to be met by the mirror surfaces. Both, in-field stray light as well as out-of-stray light have been modeled. In summary, the simulation yielded about 0.1% in-field stray light, 0.01% out-of-field stray light, 0.16% due to particle scatter and 0.2% due to scratches and digs. Summing up this results in about 0.5% thus meeting the requirement of having below 1% total scatter. The micro-roughness of the polished mirrors was checked by means of micro-interferometry. To this end, 4 different areas have been investigated with two magnifications 2.5x and 40x. In accordance with the specification, rms-values below 2 nm could be achieved for both mirrors. An example for M1 is shown in figure 11.

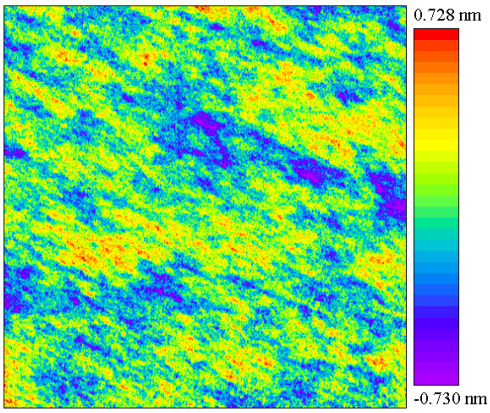

Figure 11: Surface roughness plot of M1

4. OPTO-MECHANICAL DESIGN

The optical instruments onboard of Solar Orbiter must survive extreme temperature changes as well as strong vibration and shock loads during launch, cruising and orbit. The mission is planning to approach the sun as close as 0.28 astronomic units at perihelion. In order to function under these harsh conditions, the instrument must be operational within the temperature range of-30°C to +90°C and withstand a shock load of 1500 g at launch. A robust mechanical design was developed to meet these needs and over all to guarantee a supreme optical performance under the extreme conditions in orbit. Due to the combination of extreme temperatures and strong loads, a bipod clamping was preferred over glue solution to secure the mirrors to the structure.

4.1. M1 mirror cell

The mount for M1 (shown in figure 12) consists of a triangular mount which uses a series of flexures to maintain the fixed point of the mirror. The fixed point for this design is the hole at the bottom of figure 12. Because the mount is made of hardened Invar and Invar 36 and the interface is made of aluminum, there will be substantial displacement at the two non-fixed mounting points. A double plate flexure is used at these locations to reduce the stress in the mount. The beam connecting the non-fixed mounting points is stiffened by a bar on the bottom side. This is used to move the "hotspot" of the first pump eigenmode to the center of the bipod assembly.

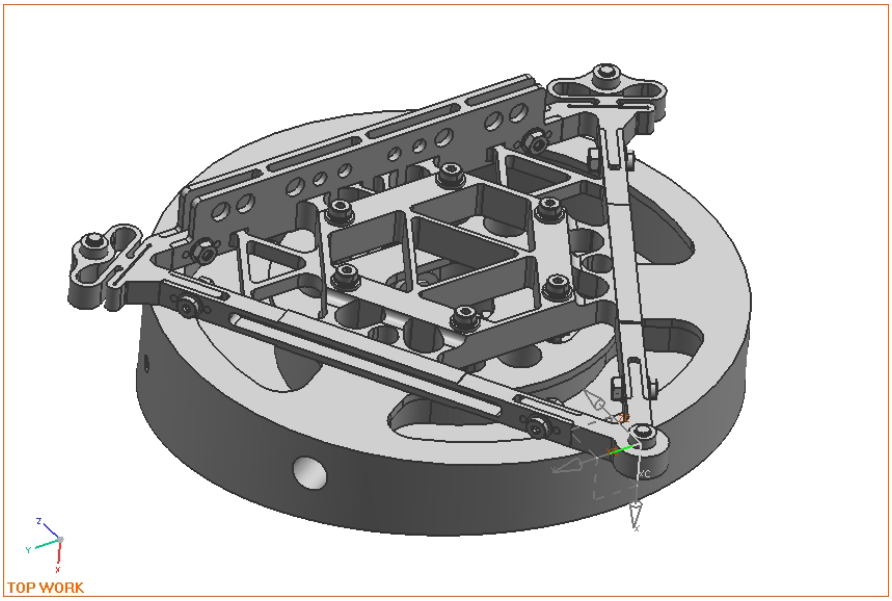

Figure 12: Layout of the M1 mirror cell

The mirror is connected to the mount by three sets of bipods, which are bolted on the mount. The mirror is secured to the bipods via an Invar pin-insert design. In order to improve the slip resistance of the mirror connection, the interface between the mirror and the pin is conical and coated with a thin gold layer. This increases the force that would be required to make the joint slip. To further increase the joint's slip resistance, an interference fit is applied in the connection between the pin and the bipod.

In order to meet the overall mass requirements and optimize the M1 cell performance, the mass of the mirror had to be reduced. The light weighting pattern was designed according to both manufacturing limitations and optical performance requirements. A minimum wall thickness of 4 mm and a minimum surface thickness of 5 mm were maintained. Undercuts were used to give the mirror extra stiffness. The final mass of the mirror anticipated due to the analysis was reduced to 827g. The light weighting design removed more mass from the side furthest from the fixed point in order to bring the center of gravity of the mirror as close as possible to the geometric center.

To minimize the thermally induced surface deformation, the mirrors were made from high quality Zerodur, while the support structure was made of a high-strength Invar alloy. Flexure connections were used to isolate the cell from the mounting plate. The uncoated mirror (compare figure 15) partially reveals its light-weighting scheme, the underlying mount structure and the bipods. A finite element (FE) model was created using NX NASTRAN v6, analyzed with the NASTRAN v. 7.1 solver, and postprocessed in NX v6 and FEMAP v10. The vibrational properties, the mechanical stability and the thermal behavior of the cells have been investigated by means of the FE-analysis. The modal analysis has been conducted in a frequency range of 0Hz to 2000Hz, covering all relevant analysis eigenfrequencies. Figure 13 shows the form of mode 1 and mode 2. The first eigenfrequency is at 251 Hz. This is above the minimum allowable eigenfrequency of 200 Hz. The second eigenfrequency (254 Hz) makes the most significant contribution to the random stresses. The extra supports at the top of the mount, shown in figure 12, were designed to increase the stiffness of the back beam and keep the "hotspot" of the eigenmode centered between the bipods.

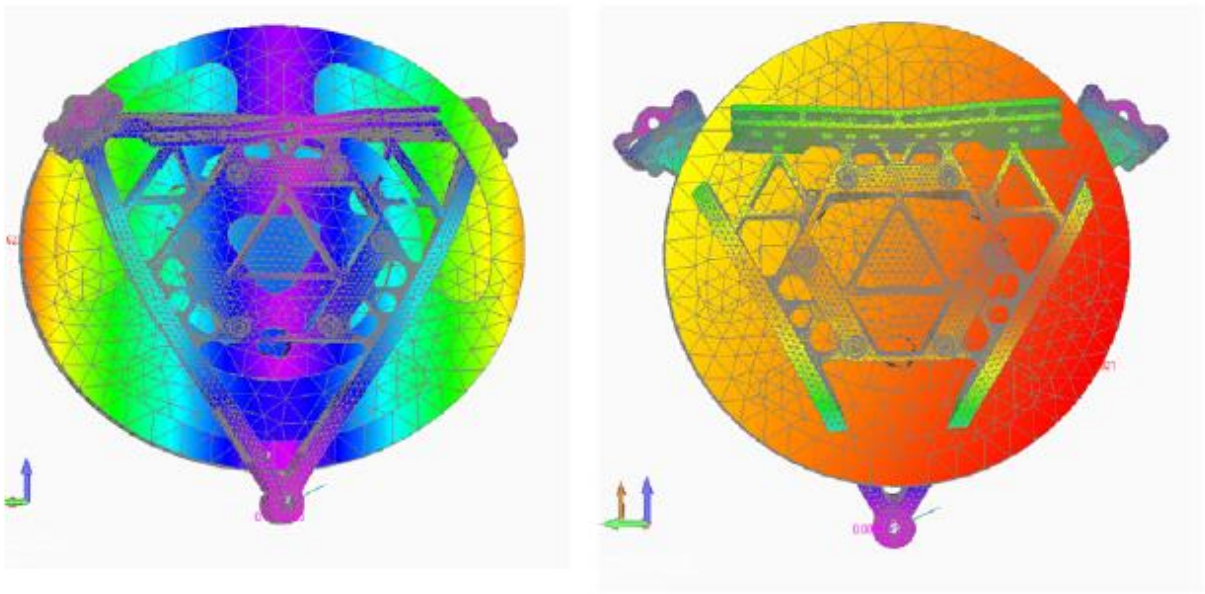

Figure 13: Resonance modes for the M1 mirror cell (FE analysis)

The mirror cell vibrations have been analyzed and tested with excitation in all three coordinate axes for random, sinusoidal and static loads. Different levels have been applied for qualification (QM) and acceptance (FM)[1]. The excitation for random vibration at qualification level in the vertical (out of plane) direction is shown in figure 14 (left). The load is equivalent to a grms-value of 15.8. The modeled response curves for all three axes are shown in figure 14 (right) where x is the vertical direction. The peak at about 250 Hz is clearly visible while the first 2 modes coincides and are hardly resolved. Similar simulations have been run for the sinusoidal and static load cases for both mirror cells. In addition, a thermo-structural analysis was run to estimate the deviation of the optical surface within the operational temperature range and at the extreme survival temperatures (-40°C and +100°C) including solar irradiation. The maximum wave-front errors are summarized in Table 1 for both mirrors.

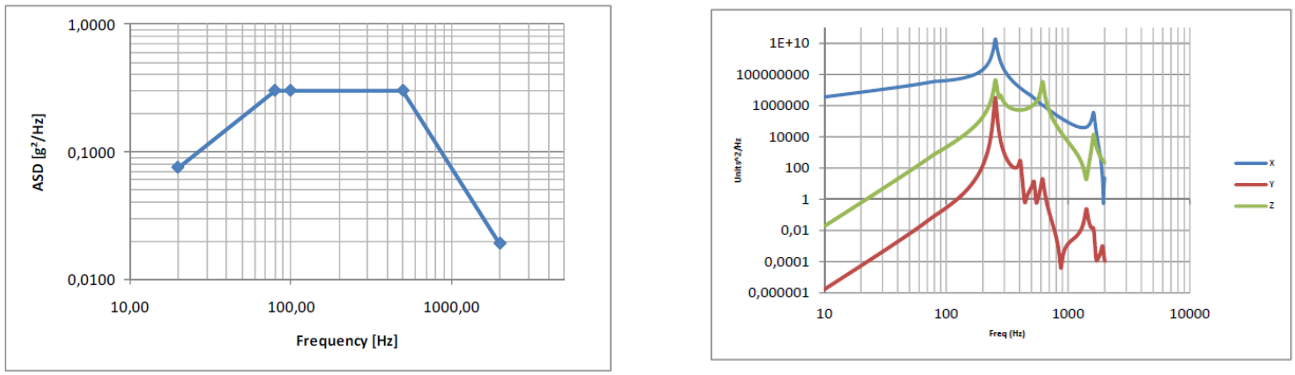

Figure 14: Excitation (left hand side) and FE predicted response curves (right hand side) for random vibration at off-axis excitation for M1

[1] The acceptence level is approximately 3dB less as compared to the qualification level

The margin of safety is a critical criterion to decide whether or not some part may withstand the forces exerted on it during operation. It is defined as follows:

$$MoS = \frac{Material\ strength}{Load \cdot FoS} - 1$$

The following factors of safety (FoS) have been applied: Zerodur (2.5), metal parts (1.5 ultimate and 1.25 yield) and fixation elements (1.4 and 1.15). The minimum MoS for all modeled load cases as described above are displayed in table 2. Even in the extreme cases, all elements show positive margins of safety which indicated that the design would withstand the loads with sufficient safety margin. Furthermore, the analysis also showed that the mirror surfaces would meet the optical requirements over the whole temperature range.

Table 2: Minimum MoS for all modeled load cases M1

	Minimum MoS	
	MoS Yield	MoS UTS
Bipods	0,13	0,35
Fixed Mount	0,05	0,25
Mount Flexures	0,18	0,40
Mount Plate	0,05	0,48
Mirror	N/A	0,23

Eventually, the FE analysis results had to be verified by means of experimental vibration tests. To this end, the mirror cells have been equipped with a set of acceleration sensors at the locations of interest. An example is shown in figure 15 for the M1 QM mirror cell. Then, a well-defined test procedure was run exposing the mirrors to the specified vibrational loads in all three axes while measuring the accelerations at well defined points.

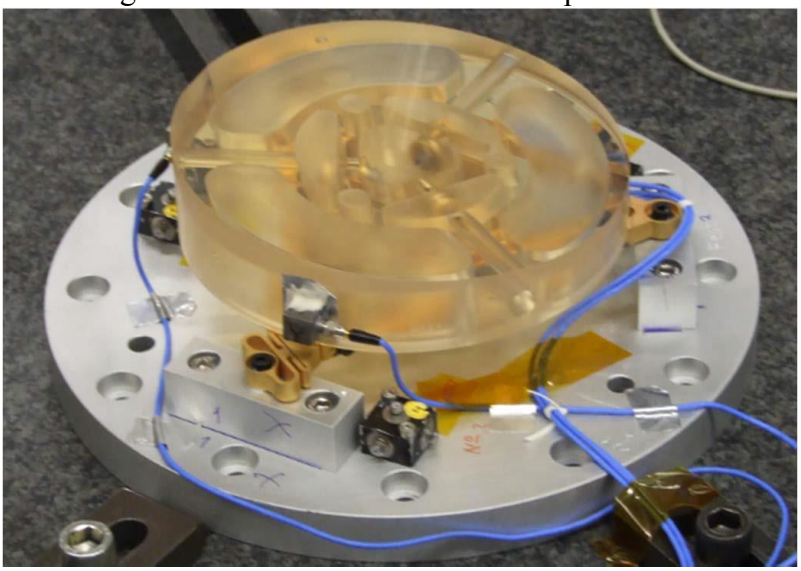

Figure 15: M1-QM cell prepared for vibration testing

To summarize the results, the QM passed the tests with success. Two experimental results are displayed in figure 16, namely the spectrum at the mirror for random excitation (left) and the sine sweep for verification (right). A closer look reveals that the first resonance is located at about 230

Hz close to the analysis results (compare figure 14). Even, a small shoulder may be seen to the left of the main peak indicating the originally two adjacent modes 1 and 2 as reported in the FE analysis (see above). Moreover, an excellent agreement can be seen comparing the sine sweep before and after the application of the maximum loads. Thus, clear evidence is given that no mechanical change (cracks, plastic deformations, slipping, loosening or other damages) have occurred.

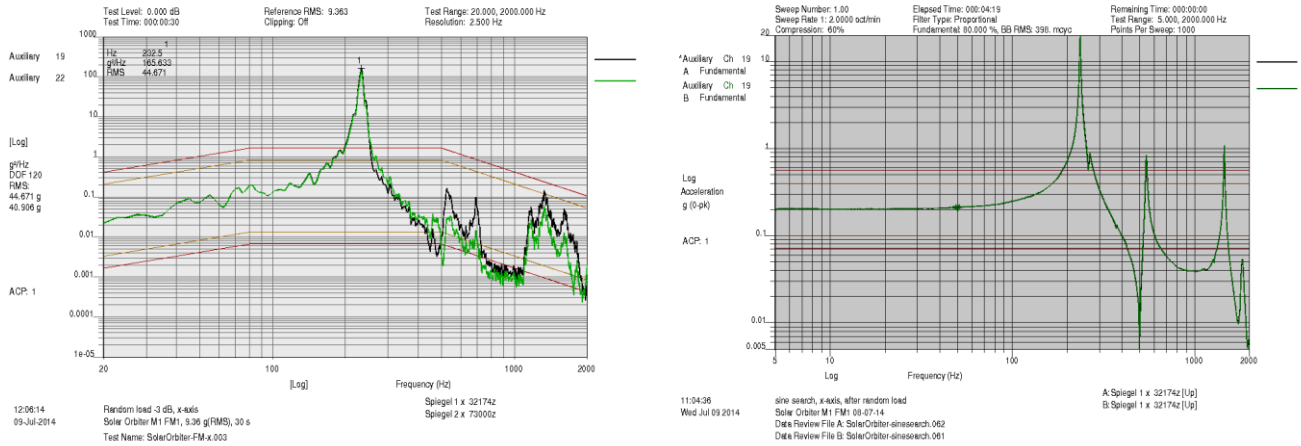

Figure 16: Measured Spectrum for random vibration (left) and sine sweep comparison (right) for the M1 QM

4.2. M2 mirror cell

The M2 cell (see Figure 17) is mounted onto a titanium ring (not shown). An invar adapter is used as a buffer between the bipods and the titanium. The bipods are secured to the mirror by invar pins. A preload is applied by a set of spring washers to maintain the connection against sliding and gapping. In order to improve the slip resistance of the mirror connection, the interface between the mirror and the pin is conical. This increases the force that would be required to make the joint slip. A spring washer is positioned between the bipod face and the mirror spacer. It is specified that the hardened invar ring and the titanium mount should not form a tight fit. Therefore, space was designed between them. However, it turned out that this space had some serious impact on the surface deformation when the rings are mounted together (see error budget for

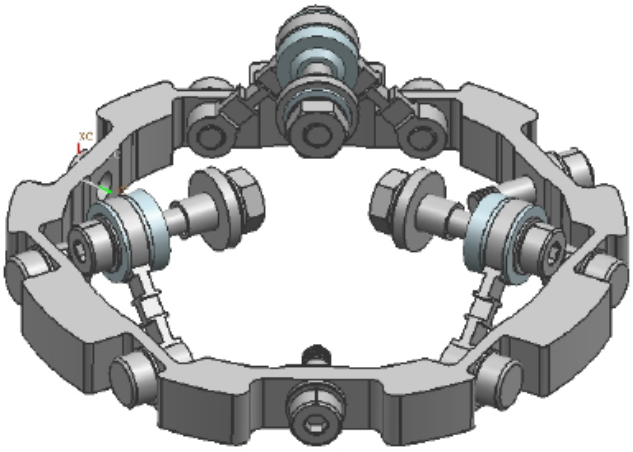

Figure 17: Lay-out of the M2 mirror cell mount

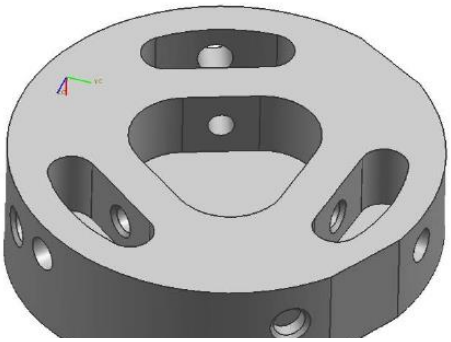

Figure 18: Light weighting of M2

M2 in Table 1). Therefore, it was decided to reduce the space and to fit the rings to each other during manufacturing. This will create a preload during tightening. The M2 cell serves as tip-tilt mirror to correct for image vibrations occurring during the flight. To this end, the complement Titanium ring is connected with a piezo drive. A light weighting was also applied to the M2 mirror (shown in figure 18). The mass without the interface plate is 69g and with the requirement defining a maximum mass of 100g is met.

The modal analysis for the M2 cell predicts the first two resonance modes at 1730 Hz and 1735 Hz thus meeting the requirement of being above 1.5 kHz. The first resonance mode is displayed in figure 19. In analogy to M1, comprehensive FE analysis have been run for the M2 cell. Again, the minimum MoS for all modeled cases (vibration loads, thermo-structural) showes positive margins of safety which indicated that the design would withstand the loads. Furthermore, the analysis also showed that the mirror surfaces would meet the optical requirements over the whole temperature range and after gravity release.

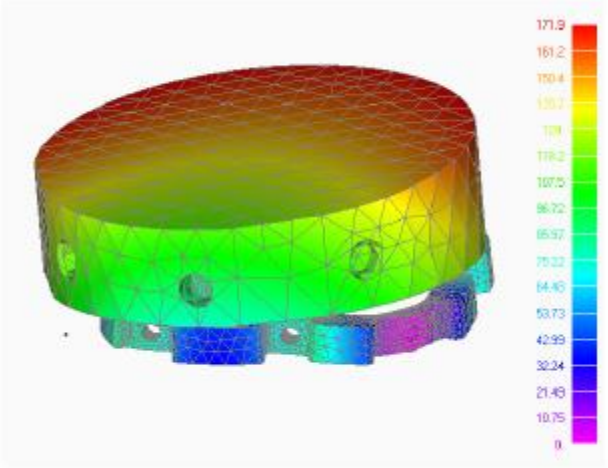

Figure 19: First resonance mode for M2

Just like the M1 cells, the M2 cells had also to undergo elaborative optical, environmental and mechanical tests to prove the appropriateness of the design and the adequate manufacturing and assembling. The simulated and measured vibration response are opposed in figure 20 (compare the red curve of the prediction with the green curve in the measurement). The first resonance was found at 1530 Hz which is slightly less than predicted but still in-spec.

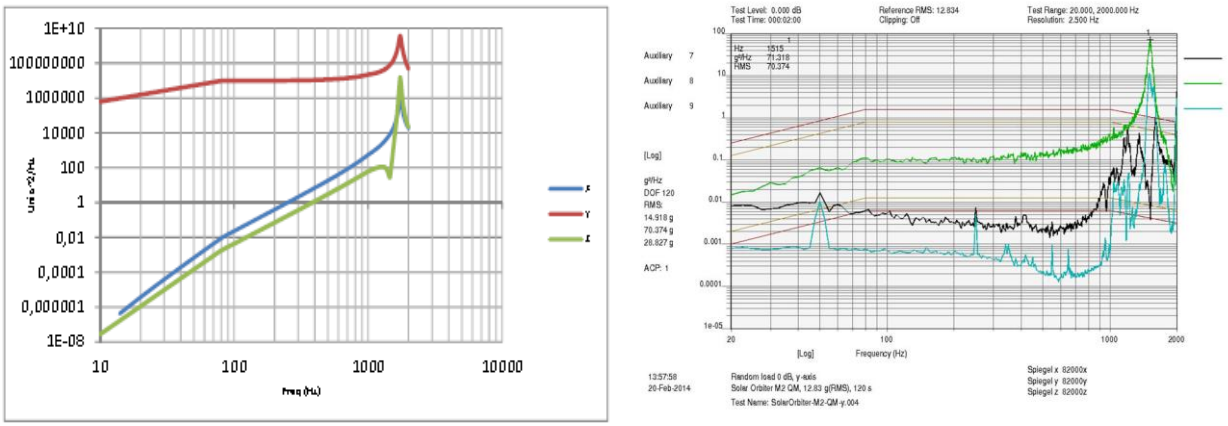

Figure 20: Predicted (left hand side) and measured (right hand side) vibration response spectrum for the M2 cell (y-axis)

4.3. Additional experimental tests

A highly precise coordinate measurement of all critical parts performed before and after the vibration test did not show any deformation beyond permission. In addition a thermal test was done at 20 °C, 40 °C & 60 °C to test the stability of the cells under extreme temperatures. It could be shown that the shift would be below the specified ±20 µm over the whole operational range. Moreover, a thermal cycling test was run (8 cycles over the whole survival range). It was shown that the optical surface recovered to full performance. In conclusion, the QM-tests proved the robustness of the cells and confirmed the basic results of the FE analysis.

5. SUMMARY AND CONCLUSION

Important aspects of the development of the mirrors for the Solar Orbiter PHI-HRT instrument have been presented. The optical design of the Ritchey-Cretien telescope was outlined and it was shown that the manufactured high-quality mirrors will meet the desired performance. In addition, surface roughness requirements have been discussed in some detail. Last but not least, the opto-mechanical design and its realization has been sketched. Finally, it could be demonstrated by means of comprehensive experimental tests that the design is robust under the harsh environment conditions during the solar orbit and should be able to provide high quality images for solar physics research.

ACKNOWLEDGEMENTS

The authors like to thank all contributors from Cassidian Optronics, Carl Zeiss and MPS for their share in making the development a success. Particularly, the experience and skillful work of Mr. H. Merkle (CO) is highly appreciated.

REFERENCES

[1] J. C. Stover, ed., *Optical Scattering: Measurement and Analysis*, 2nd ed., Vol. PM24 of the Press Monographs SPIE, Bellingham, Wash., 1995.

[2] J. E. Harvey, “Light scattering characteristics of optical surfaces”, Proc. SPIE 107-5, 1977.

[3] R. N. Youngworth and B. D. Stone, “Simple estimates for the effects of mid-spatial-frequency surface errors on image quality”, Appl. Optics 39, p. 2198 ff, 2000.

[4] Photon Engineering FRED Software, www.photonengnr.com